Effect of Postweld Heat Treatment on the Toughness of Heat-Affected Zone for Grade 91 Steel

After investigating the impact toughness of the heat-affected zone for Grade 91 steel welds, it was discovered that 760°C for 2 h postweld heat treatment can significantly increase the cross-weld toughness of the heat-affected zone

BY B. SILWAL, L. LI, A. DECEUSTER, AND B. GRIFFITHS

ABSTRACT

The impact toughness of the heat-affected zone (HAZ) for Grade 91 steel welds has been experimentally investigated. The as-welded multipass HAZ has a significant scatter in toughness, due to variations in the Charpy notch location and the path of fracture propagation. The cross-weld Charpy specimen gives a toughness value that can be attributed to contributions by the weld metal, various HAZ regions, and the base metal. The microstructure evolution of various HAZ regions during postweld heat treatment (PWHT) has been investigated and used to explain the toughness changes. A 760°C for 2 h PWHT can significantly increase the cross-weld toughness of the HAZ. The measured weld HAZ toughness can be understood using a linear additive model that employs as the inputs the toughness values of various HAZ regions reproduced on the Gleeble®. The toughness of the coarse-grained heat-affected zone (CGHAZ) recovers the slowest as a function of increasing PWHT temperature, and remains low until a 730°C heat treatment. To guarantee an adequate HAZ toughness, a PWHT of at least 730°C is recommended. Postweld heat treatment above the A_{C1} temperature will result in the formation of fresh martensite, which decreases the toughness and increases the hardness of all HAZ regions. Postweld heat treatment 20°C below the A_{C1} temperature for 2 h has produced the highest toughness and lowest hardness of all HAZ regions.

Introduction

Grade 91 steel, known as the modified 9Cr-1Mo-V, designated as P91 for pipe and plate (ASTM A335 P91), and T91 for tube (ASTM A213 T91), is a creep-enhanced ferritic steel that has been widely used in power-generating applications as a header, superheater, and reheater. Initially developed by Sikka et al. (Ref. 1), the alloy was to have an improved strength and toughness for liquid metal fast breeder reactor. Then the alloy was modified by adding vanadium, nickel, aluminum, niobium, and nitrogen to become the modified 9Cr-1Mo-V steel. Properties such as high thermal conductivity, better resistance to stress corrosion cracking, lower thermal expansion coefficient, and high resistance to thermal fatigue made Grade 91 a better replacement for lower alloy steels for piping and vessels. With superior mechanical properties such as yield, ultimate tensile, and creep rupture strengths matching or exceeding that of 9Cr-1Mo, 2¼Cr-1Mo, HT9, EM12, and 304 stainless, Grade 91 was identified (Ref. 2) as a material of choice in the petrochemical and nuclear industry.

The as-received material of Grade 91 undergoes normalizing-and-tempering heat treatment to achieve better mechanical properties. The ASME code requires that the steel be normalized at 1038°–1149°C and tempered at a minimum temperature of 732°C. A fully tempered martensite matrix, with finely dispersed carbides, and carbo-nitrides precipitation on the grain boundaries, is the typical microstructure. The carbides are of $M_{23}C_6$-type, M being metallic elements, mainly Cr and Fe, Mn, and Mo if present; and the grain boundary carbonitrides are of MX-type, M being Nb and V, and X being C and N (Ref. 3).

When the as-received material undergoes manufacturing processes such as welding, the mechanical properties will change due to phase transformations, including the formation of fresh martensite. It becomes necessary to conduct a postweld heat treatment (PWHT) below the A_{C1} temperature for some period of time to temper the martensite and achieve the desired microstructure and mechanical properties. Because the degree of martensitic hardening depends upon the material chemical composition and welding conditions, the correct control of time and temperature for the PWHT becomes critical. Instead of only performing tempering, it would be better to do both normalizing and tempering after welding to achieve better creep properties as suggested by Santella et al. (Ref. 4).

The impact toughness as influenced by PWHT becomes important when controlling the delayed weld cracking during manufacturing, the room-temperature pressure testing, and startup of a unit after installation and maintenance. Although various papers have been published on impact toughness of the weld metal Grade 91 (Refs. 5–7), the toughness of the heat-affected zone (HAZ) has not been studied in detail. The objective of this paper is to study the impact toughness of the HAZs in Grade 91 joints as affected by PWHT both below and above the A_{C1} temperature.

KEYWORDS

Heat-Affected Zone (HAZ)
Grade 91
Postweld Heat Treatment (PWHT)
A_{C1} Temperature

Experimental Procedure

Welding and Heat Treatment

ASTM A335 P91/ASME SA335 P91 pipe

B. SILWAL, L. LI (leijun.li@usu.edu), *A. DECEUSTER, and B. GRIFFITHS are with the Department of Mechanical & Aerospace Engineering, Utah State University, Logan, Utah.*

Presented during the AWS Professional Program at FABTECH 2012, Las Vegas, Nev.

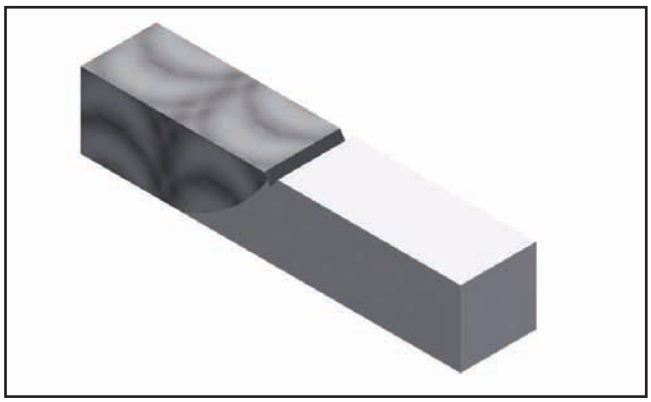

Fig. 1 — Schematic of the Charpy coupon extraction and location of the notch relative to the weld metal on the left and HAZ in the base metal.

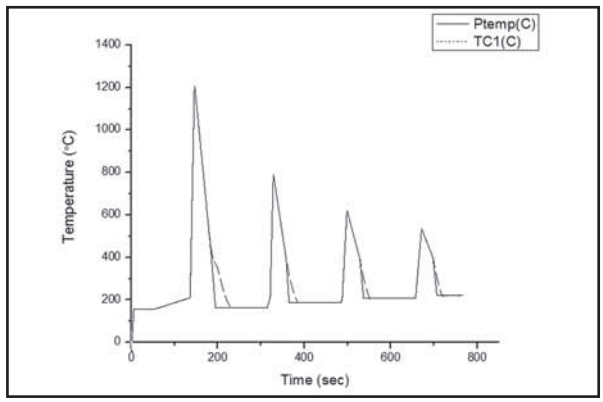

Fig. 2 — Measured and Gleeble®-simulated thermal cycle for the CGHAZ. P_{temp} is programmed temperature that duplicates the measured temperature, and TC1 is the actual temperature achieved in the specimen on the Gleeble®.

was used as base metal. The as-received pipe had an 8.625 in. (219 mm) outer diameter, 1.143 in. (29 mm) thickness, and was normalized for 8 min at 1060°C and tempered for 45 min at 786°C. The chemical composition of the material is given in Table 1.

Two 5-in.- (127-mm-) long pipes were welded together by gas tungsten arc welding (GTAW) and flux cored arc welding (FCAW) processes. The double-V weld groove had a 60-deg included angle with a 1.5-mm root face. The same process was repeated eight times to conduct a full factorial design of the welding process parameters of maximum and minimum preheat temperature, interpass temperature, and heat input (as mentioned maximum being high and minimum being low hereafter). Gas tungsten arc welding was used for the root pass with 300 A DC and 1.27 m/min wire feed speed, and FCAW was used for the filling passes with 26.1 and 27 V arc voltage and 6.35 and 7.62 m/min wire feed speed. The 0.14 m/min linear travel speed was maintained by a stepper motor controlled fixture. Pure argon shielding was used for GTAW and mixed 75/25 argon/CO_2 shielding was used for FCAW. The filler metal was 1.2-mm-diameter ER90S-B9 for GTAW, and ER91T1-B9 for FCAW. The linear travel speed was 0.292 m/min.

Sixteen Type-K thermocouples were placed on different locations from the edge of the weld groove to measure the temperature profile. Two 8-channel data loggers were used to record the temperature measurements with a sampling frequency of 5 Hz. After welding, the locations of the thermocouples were remeasured relative to the weld interface line, which was assumed to have experienced the melting temperature. The microstructure from the HAZ of the as-welded specimen was then analyzed, and the HAZ locations were identified and measured from the weld interface. For instance, the intercritical heat-affected zone (ICHAZ) was identified to be about 2.1 mm from the weld interface for weld #5. The thermocouple located at or near 2.0 mm from the weld interface was then identified as that representing the ICHAZ thermal cycle.

The interpass temperature was also maintained with the use of a ceramic pad heater and surface temperature probe

Table 1 — Chemical Composition of Grade 91Base Material and Filler Metals (wt-%)

	ER90S-B9 GTAW	E91T1-B9 FCAW	Base Metal
C	0.097	0.1	0.11
Mn	0.56	0.79	0.37
Si	0.25	0.28	0.37
S	0.004	0.008	0.002
P	0.006	0.02	0.016
Cr	8.83	9.1	8.47
Ni	0.307	0.55	0.08
Mo	0.928	0.88	0.94
Nb	0.064	0.03	0.071
N	0.03	0.05	0.0476
O_2	47 ppm		
Ti	0.001		
Al	0.002	0.001	0.002
V	0.197	0.2	0.19
Cu	0.013	0.04	
As	0.003	0.002	
Sn	0.003	0.008	
Sb	0.003	0.002	
B	0.0007		
Zr	0.001		
CO	0.028		
Ca	0.003		
Ta	0.001		
W	0.005		
H_2	3 ppm		
Ni+Mn	0.867	1.34	

Table 2 — Average Impact Energy Values for Various Simulated HAZs, and the Base and Filler Metals in Both the As-Welded and Heat-Treated Conditions

Condition	As-welded (J)	PWHT: 760C-2H (J)
Base Metal (BM)	229	242
Weld Metal (WM)	7	56
CGHAZ	10	184
FGHAZ	75	246
ICHAZ	180	239

Weld Test #	Preheat (°C)	Inter-pass (°C)	Heat input
1	250	300	0.9986kJ/mm (WFS 7.62m/min @ 27V)
2	250	300	0.8655kJ/mm (WFS 6.35m/min @ 26V)
3	250	200	0.9986kJ/mm (WFS 7.62m/min @ 27V)
4	250	200	0.8655kJ/mm (WFS 6.35m/min @ 26V)
5	150	300	0.9986kJ/mm (WFS 7.62m/min @ 27V)
6	150	300	0.8655kJ/mm (WFS 6.35m/min @ 26V)
7	150	200	0.9986kJ/mm (WFS 7.62m/min @ 27V)
8	150	200	0.8655kJ/mm (WFS 6.35m/min @ 26V)

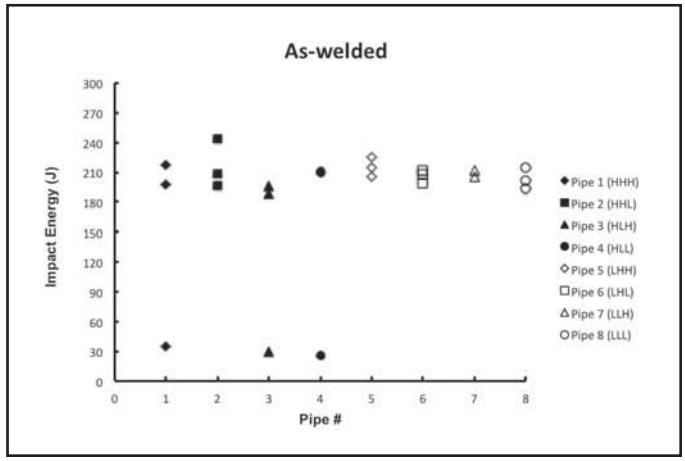

Fig. 3 — Charpy impact test results from specimens in the as-welded condition for different welding parameters.

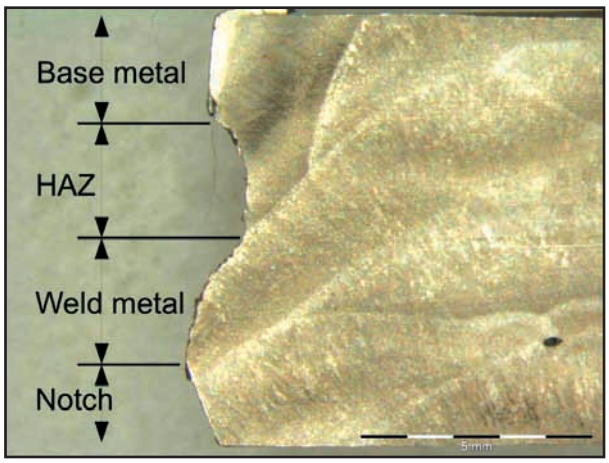

Fig. 4 — Fracture path of an example of Charpy impact-tested, as-welded specimen. The fracture originated from the notch (in the lower-left corner), passed through the weld metal, HAZ, and base metal.

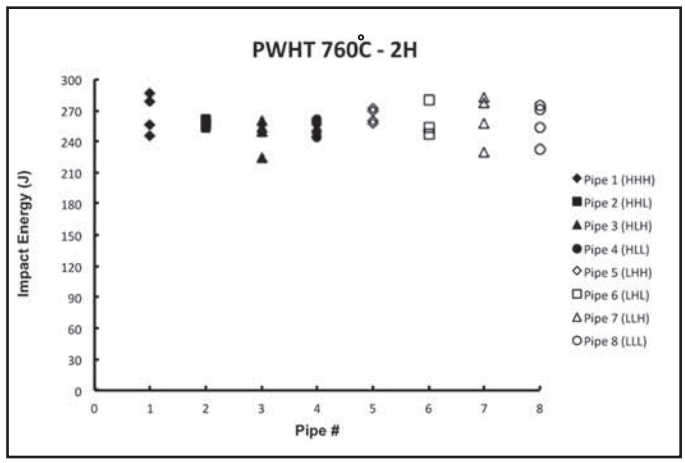

Fig. 5 — Charpy impact test results for joints heat treated at 760°C for 2 h. The joints were made using different welding parameters.

with an accuracy of temperature control at ± 10°C. The preheat temperature before welding was between 150° and 250°C. The interpass temperature during welding was between 200° and 300°C. A pneumatic descaler and wire brushing were used for slag removal. A postweld bake-out at 250°C temperature for 4 h was conducted with temperature-controlled ceramic heat pads. Subsequently, the as-welded joints were PWHT in a furnace for 2 h at various temperatures.

Impact Test

Charpy impact specimens were extracted in the pipe's longitudinal direction from the middle thickness of both the as-welded and PWHT joints. Standard Charpy impact V-notch specimens (10 × 10 × 25 mm) were prepared according to ASTM A370 (Ref. 8). All specimens were macroetched to reveal the fusion boundary, which served as the location for the notch so that the fracture path would traverse the HAZ — Fig. 1. Three specimens in the as-welded condition and four specimes in the PWHT condition were impact tested at room temperature. Standard metallographic procedure was followed to prepare the specimens for optical microscopy. The polished specimens were etched with the Nital (10% nitric acid in methanol) or Le Pera reagent (4% picric acid in ethanol mixed with a 1% sodium metabisulfite in distilled water in an 1:1 volume ratio) to analyze the microstructure.

Microstructure Simulation

To "magnify" the small HAZ regions so that large samples of similar microstructure can be tested, a Gleeble® 1500D was used to simulate the multipass welding process. The measured thermal cycle for each individual HAZ was reproduced in three smooth Charpy specimens. As an example, the thermal cycle for the as-welded coarse-grained heat-affected zone (CGHAZ) is shown — Fig. 2. The simulated samples were then heat treated at different temperatures from 600° to 840°C with a temperature difference of 40°C. Notches were machined in the middle of the test specimens. Two specimens for each tempering temperature were tested and both results were reported.

The average energy values for these "pure" metals (of the simulated HAZ regions, fusion zone, and base metal) are listed in Table 2. This method of creating simulated samples by using the thermal cycle is different from most previous studies, because not only the first peak temperature but also the subsequent temperature peaks by multipasses were applied to achieve similar properties of the as-welded samples. The transformation temperatures A_{C1}, A_{C3}, M_s, and M_f temperature for the Grade 91 base metal were also measured using dilatometry on the Gleeble®. The specimen was heated at a rate of 100°/min from room temperature to 728°C, then the heating rate was switched to 28°/h to heat to 1300°C, at which point the specimen was allowed to naturally cool to room temperature. A precise extensometer measured the diameter change

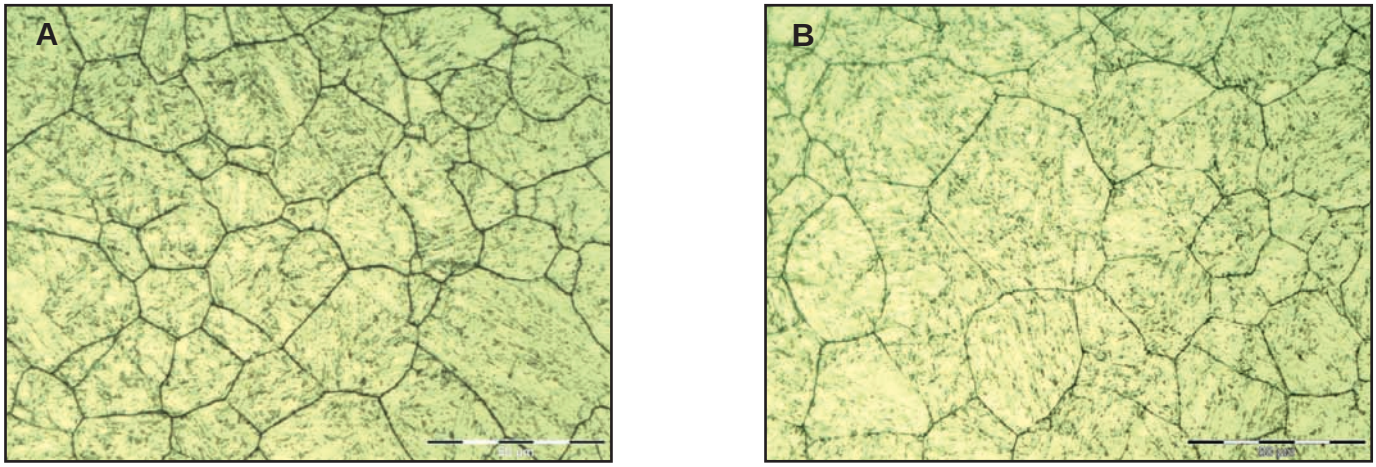

Fig. 6 — A — Microstructure of the CGHAZ from weld test #5; B — the corresponding simulated multipass CGHAZ microstructure. Nital etching.

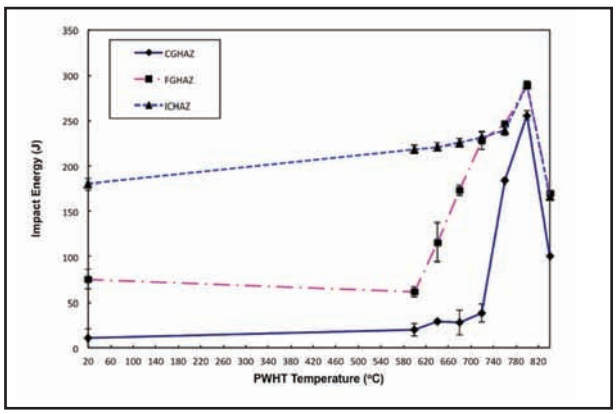

Fig. 7 — Charpy impact energy results of different HAZs after PWHT at various temperatures for 2 h.

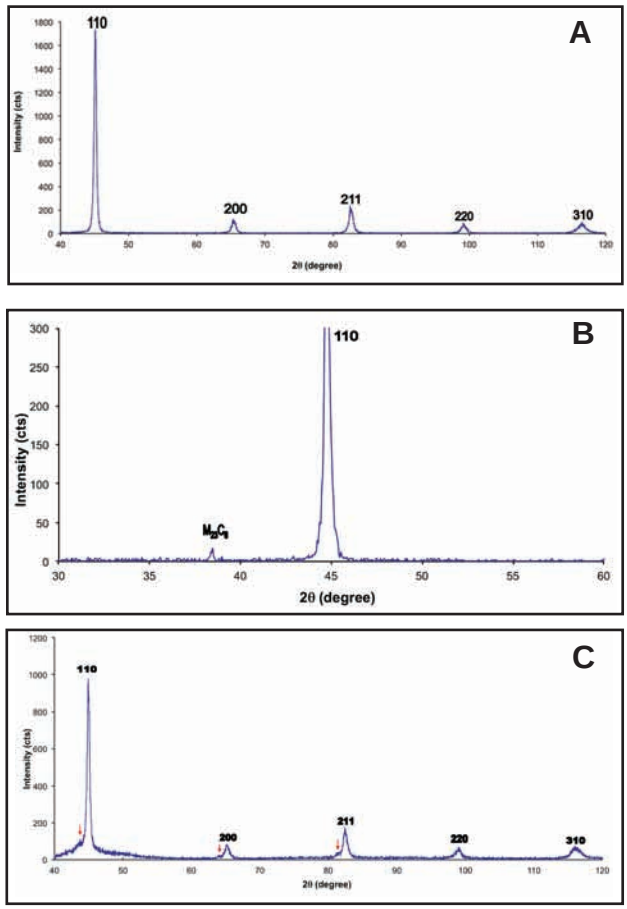

Fig. 8 — A — XRD spectrum of the as-received base metal Grade 91; B — magnified lower 2θ angle portion showing an $M_{23}C_6$ carbide peak; C — XRD spectrum of a specimen air-cooled from 840°C, showing broadening of peaks, indicated by the arrows, due to fresh martensite.

during the entire heating and cooling process.

Results and Discussion

Toughness of the HAZ

The impact energy values for the HAZs in the as-welded samples are shown in Fig. 3. The average impact energy exceeds 180 J for the as-welded samples. The difference in impact energy values with different process parameters during welding is not significant, although a greater preheat temperature (250°C) seems to have produced wider scatter in impact energy of the HAZ. Lower preheat (150°C) seems to have produced a much narrower scatter band in impact energy of the HAZ. A few as-welded samples have impact energy values close to 30 J.

An inspection of the fracture path reveals the propagation of fracture in these low toughness specimens originates from the notch and passes through the weld metal, HAZ, and base metal — Fig. 4. The weld metal in the as-welded condition has an impact energy of 7 J. Clearly, the measured impact energy is a sensitive function of the position of the notch for the heterogeneous weld joint. Similar observations have been made by other researchers, such as Moitra et al. (Ref. 10) and Jang et al. (Ref. 11), in a study of the effect of notch location on impact toughness of weld metal and HAZ.

After a PWHT at 760°C for 2 h, the impact energy of all HAZ specimens has increased consistently — Fig. 5. The minimum energy level for joints made using different welding parameters is 220 J. The wide scatter of impact energy levels for the as-welded weld HAZ has been narrowed down. An inspection of fractography of tested specimens revealed the fracture paths to be consistently starting from the notch, traversing the HAZ and base metal. None of the fracture paths in the heat-treated samples has deviated into the weld metal, which after the 760°C for 2 h heat treatment, has the impact toughness increased from 7 to 56 J.

Contribution to Toughness by Individual Zones

The Gleeble®-simulated microstructure is verified to be similar to that from the

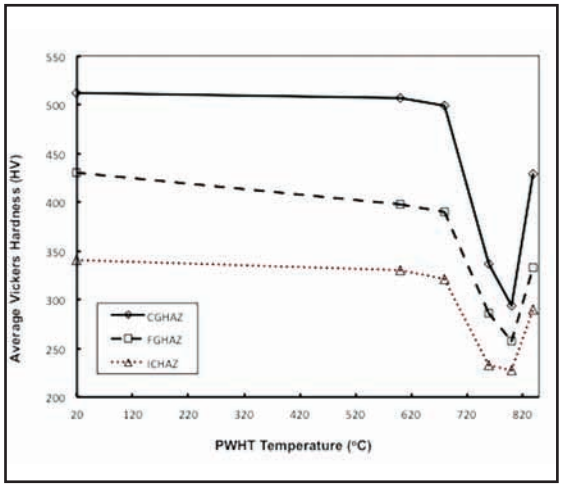

Fig. 9 — Average Vickers hardness values of different HAZ zones after PWHT at various temperatures for 2 h.

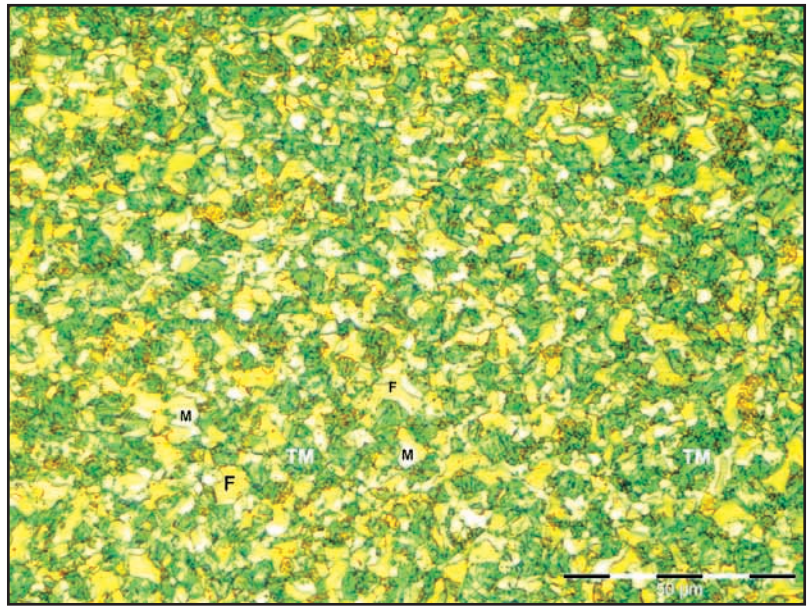

Fig. 10 — The microstructure of ICHAZ heat treated at 840°C for 2 h and air cooled. Etched with Le Pera reagent, the microstructure constituents include white-etching martensite (M), tan-etching ferrite (F), and dark-etching tempered martensite (TM).

HAZs of the welded samples. An example comparison of microstructures for the CGHAZ is shown in Fig. 6. The two microstructures not only share the same grain size, but also the martensitic substructure, size, and amount of carbide particles. Such simulated microstructure for the entire cross-section of the Charpy specimen enables an accurate evaluation of impact toughness of individual HAZs.

The Charpy impact results of the simulated HAZ samples heat treated at various temperatures for 2 h are shown in Fig. 7. Among the three HAZ regions, the ICHAZ exhibits the highest toughness, while the CGHAZ has the lowest toughness and fine-grained heat-affected zone (FGHAZ) has an intermediate toughness. The CGHAZ exhibits the lowest impact energy following a 600°C, 2-h heat treatment. This low toughness remains until the PWHT temperature is at 720°C. The impact energy of CGHAZ then increases significantly when the PWHT temperature is 760°C. A PWHT at 800°C results in the peak toughness for the CGHAZ. The impact toughness then decreases when the PWHT temperature is 840°C. The ICHAZ toughness remains at 220 J for PWHT temperatures below 760°C, and reaches the peak value following an 800°C heat treatment. The ICHAZ toughness also decreases when the PWHT temperature is 840°C. The FGHAZ toughness increases with a higher PWHT temperature between 600° and 720°C. After the 720°C PWHT, the FGHAZ toughness has increased to the same level as that of the ICHAZ. Further increases in the PWHT temperature from 720°C result in the exact same toughness for both the FGHAZ and ICHAZ. A notable trend is that all HAZ regions reach the peak toughness following an 800°C PWHT; and all HAZ regions lose toughness following an 840°C PWHT.

Table 3 — Sample Calculation of Contributions of Base Metal and HAZ to the Total Impact Energy

	As-welded	PWHT: 760C-2H
L_{CGHAZ} (mm)	0.5	0.7
L_{FGHAZ} (mm)	0.7	0.8
L_{ICHAZ} (mm)	0.3	0.5
L_{BM} (mm)	6.0	6.0
E_{CGHAZ} (J)	0.6	16
E_{FGHAZ} (J)	9	24
E_{ICHAZ} (J)	6	15
E_{BM} (J)	203	187
E_{Calc} (J)	220	243
E_{Exp} (J)	210	257
Difference (%)	–5	5

The L_{CGHAZ} value is the measured fracture length, E_{CGHAZ} value is the calculated contribution to impact energy by CGHAZ, E_{Calc} is calculated total impact energy, and E_{Exp} is the measured total impact energy from the welded sample.

The measured impact toughness reported in Fig. 5 represents the total energy for the fracture to traverse the entire specimen. The fracture path may have traversed the weld metal, various HAZ zones, and the base metal. As a first approximation, we can consider the total impact energy (E_{Calc}) to be consisted of a linear summation of contributions by various zones as follows:

$$E_{Calc} = (E_{CGHAZ} + E_{FGHAZ} + E_{ICHAZ}) + E_{WM} + E_{BM} \quad (1)$$

where E_{CGHAZ} is the energy contribution of the CGHAZ, E_{FGHAZ} is the energy contribution of the FGHAZ, E_{ICHAZ} is the energy contribution of the intercritical HAZ, E_{WM} is the energy contribution of the weld metal, and E_{BM} is the contribution of the base metal.

Because the Charpy specimen has a uniform width, the contribution of individual zones to the total Charpy impact energy can be calculated using the measured fracture length in each zone. For example, for the contribution of base metal (E_{BM}) to the total impact energy, the following formula can be used:

$$E_{BM} = \left(\frac{L_{BM}}{L_{Total}}\right) E'_{BM} \quad (2)$$

where L_{BM} is the length of the fracture path that falls in the base metal, L_{Total} is the total length of the fracture path of the Charpy specimen, and E'_{BM} is the measured impact energy of the "pure" base metal. Similar definitions can be made for E_{CGHAZ} for the CGHAZ, E_{FGHAZ} for the FGHAZ, and E_{ICHAZ} for the ICHAZ, re-

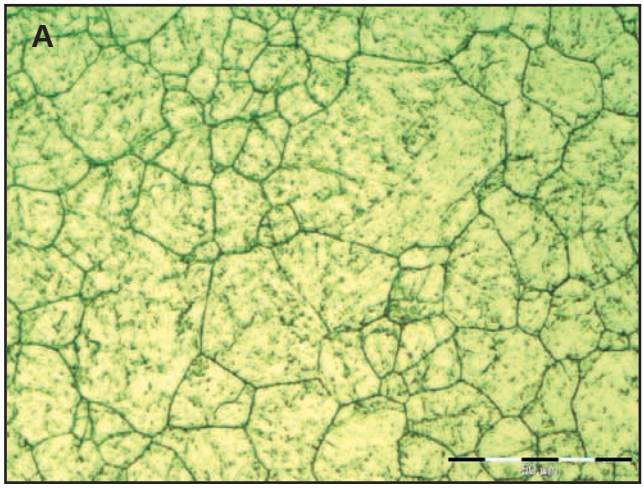

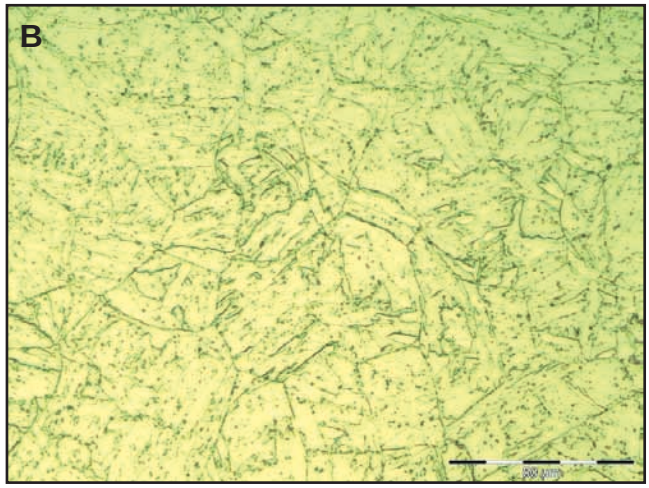

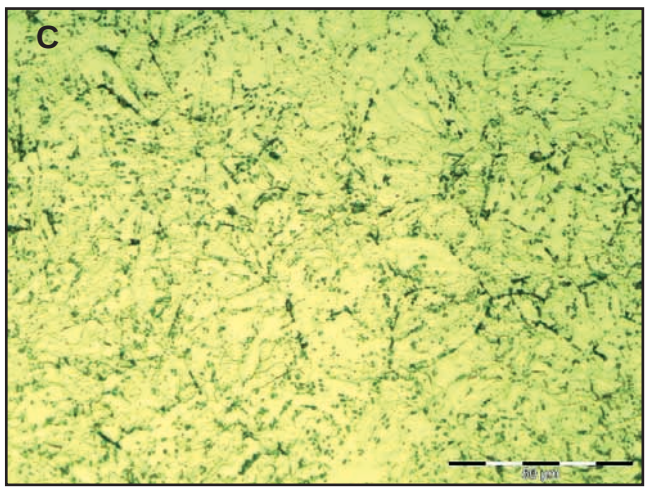

Fig. 11 — Microstructure of CGHAZ after heat treatment at the following for 2 h: A — 640°C; B — 800°C; C — 840°C. Nital etching.

spectively. Experimentally measured impact toughness data from the simulated HAZ, base metal, and pure weld metal are listed in Table 2 for the as-welded and 760C-2H heat-treated conditions.

Tested Charpy toughness specimens were polished and etched to reveal the microstructure along the fracture path as shown in Fig. 4. Measurements of the length of fracture path that falls in each microstructure zone were taken. Sample calculations to predict the total Charpy impact energy are shown (Table 3). Impact energy data shown in Table 2 and measured fracture length fractions are used as input parameters for the calculations. Compared with the experimental impact energy value (E_{Exp}), the calculated total energy (E_{Calc}) is within ±5% difference. Using this linear summation method, a cross-weld HAZ toughness test result can be understood if the test specimen is measured metallographically for the fracture length and toughness of individual HAZ zones are determined.

Evolution of Microstructure during PWHT

The as-received material of Grade 91 has undergone a normalization at 1060°C and tempering at 786°C. The as-received microstructure consists of fully tempered martensite and ferrite along with finely dispersed $M_{23}C_6$-type carbide. Figure 8A and B show the XRD analysis of the as-received material, indicating the ferritic (*bcc*) crystal system for the tempered martensite and existence of $M_{23}C_6$-type carbide.

The transformation temperatures identified by dilatometry for slow heating and air cooling are A_{C1} = 818, A_{C3} = 925, M_s = 394, and M_f = 230°C for the as-received base material. The equilibrium A_1 temperature based on Mn and Ni content is also estimated using the following formula (Ref. 12)

$$A_1(°C) = 845.5 - 43.9\,(Mn + Ni) - 9\,(Mn + Ni)^2 \quad (3)$$

and found to be 822°C, which is very close to the slow-heating A_{C1} identified by dilatometry. If the PWHT temperature is above the A_{C1} temperature, austenite will start to form, which on-cooling will transform to fresh martensite. A reduction in toughness will be observed because of such untempered martensite. Figure 7 shows the significant reduction in the measured toughness for all HAZ regions following an 840°C PWHT. Since 840°C is above the A_{C1} temperature, this toughness reduction is due to martensite formation. Figure 8C provides the evidence of martensite formation in a specimen air cooled from 840°C. Fresh martensite and tempered martensite in Grade 91 share most of the XRD signatures, except the subtle broadening of the peaks near their bases (Ref. 3). Comparison of Fig. 8A and C does show a broadening of peak bases due to fresh martensite. The arrows in Fig. 8C indicate the traces of fresh martensite in the specimen.

Further evidence of fresh martensite formation for PWHT at temperatures higher than the A_{C1} is provided by the hardness of microstructure. Figure 9 shows the changes in hardness of various HAZ regions as a function of the PWHT temperature. Because the microstructure is heterogeneous, a 1000-g load has been used during the Vickers hardness measurements to maximize the indentation size, so that an "average" hardness is obtained. Compared with the toughness results shown in Fig. 7, the hardness curves show an inverse trend as a function of the PWHT temperature — the minimum hardness at 800°C PWHT corresponds to the maximum toughness. The significant increase in hardness following the 840°C PWHT can be attributed to the fresh martensite. Microstructural evidence for martensitic transformation for PWHT above the A_{C1} temperature is available after etching the specimens with the Le Pera regent, which reveals the fresh martensite in white, ferrite in tan, and tempered martensite and bainite in a dark color (Ref. 9). In Fig. 10, the microstructure of ICHAZ following an 840°C, 2-h PWHT is shown to contain approximately 15 vol-% fresh martensite, 25 vol-% ferrite, and 60 vol-% tempered martensite.

The CGHAZ has experienced a peak temperature between 1100°C and the melting temperature of 1382°C, during which there is a complete dissolution of carbides and significant grain growth of the high-carbon and high-alloy-containing austenite. Fresh martensite that forms upon cooling is strong and brittle. Although it has been tempered by subse-

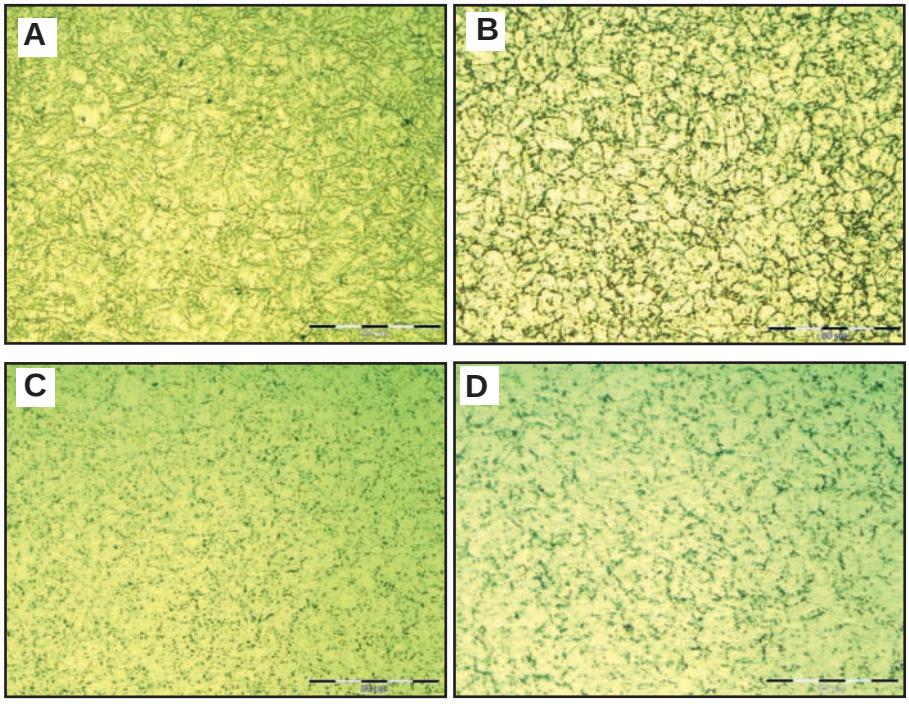

Fig. 12 — Microstructure of FGHAZ in the following conditions for 2 h: A — as-welded; B — after heat treatment at 640°C; C — 800°C; and D — 840°C. Nital etching.

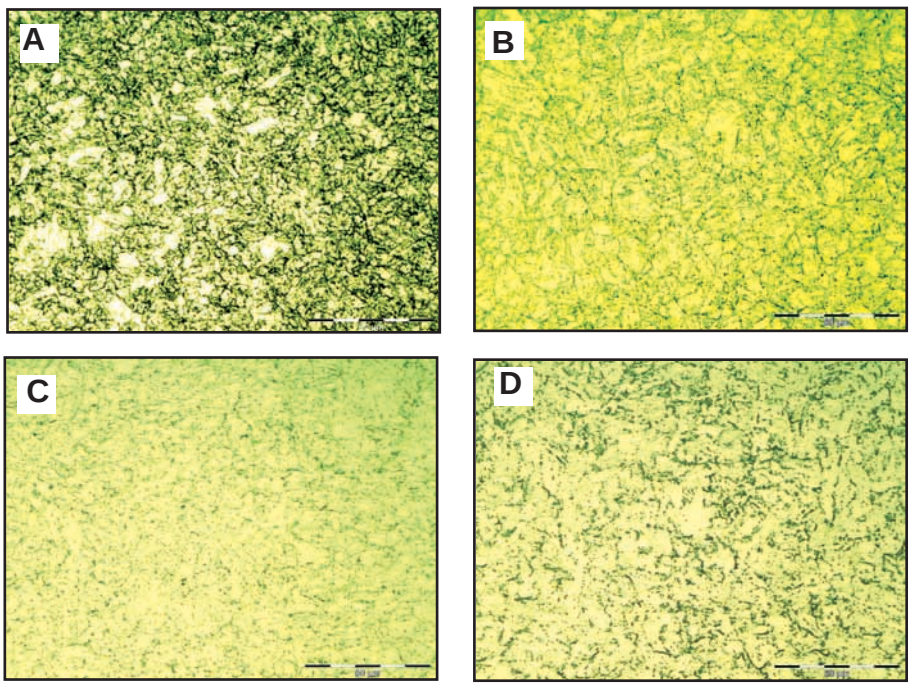

Fig. 13 — Microstructure of ICHAZ in the following conditions for 2 h: A — As-welded; B — after heat treatment at 640°C; C — 800°C; D — 840°C. Nital etching.

quent thermal cycles in the multiple welds, the tempered martensite microstructure in the CGHAZ is still brittle — Fig. 6. With a PWHT at 640°C, more tempering of martensite has occurred, but the microstructure is virtually identical with that of the as-welded CGHAZ — Fig. 11A. Therefore, the toughness of CGHAZ remains low until the PWHT temperature is further increased to above 720°C — Fig. 7. The microstructure of 800°C heat-treated CGHAZ shows the tempering of martensite to ferrite with associated carbide precipitation. Although the grain size remains the same as the as-welded condition (average 30-μm), there are new finer ferrite subgrains and annealing twins formed — Fig. 11B. The CGHAZ in this microstructure has the highest impact toughness. The PWHT at 840°C refines the grain size and coarsens the carbide particles but produces the brittle fresh martensite, as explained earlier — Fig. 11C. The toughness decreases from the 800°C PWHT value.

The fine-grained HAZ has experienced a peak temperature above A_{C3} (925°C) but below the temperature for austenitic grain growth. The austenitized FGHAZ has an average grain size of 8 micrometers that transforms to martensite on-cooling. The as-welded microstructure following multibead welding is tempered martensite — Fig. 12A. A PWHT at 640°C produces tempered martensite and some ferrite with dispersed carbide particles — Fig. 12B. Toughness is recovered to above 100 J following the PWHT at 640°C. The FGHAZ also shows the maximum toughness and minimum hardness following a PWHT at 800°C due to a microstructure of fine-grained ferrite with fine dispersed carbide particles — Fig. 12C. The PWHT at 840°C increases the grain size and coarsens the carbide particles but produces the brittle fresh martensite — Fig. 12D. The toughness therefore decreases from the 800°C PWHT value.

The intercritical HAZ has experienced a peak temperature between the A_{C1} and A_{C3}, therefore is partially austenitized on-heating. The multibead as-welded microstructure is a mixture of base metal's ferritic constituent and newly formed and tempered martensite — Fig. 13A. The 180-J toughness of ICHAZ is contributed mostly by the base metal, which has a toughness of 230 J. A PWHT at 640°C further tempers the martensite, but since the toughness is governed by the dominating base metal, no significant changes in the toughness are observed — Fig. 13B. The ICHAZ also shows the maximum toughness and minimum hardness following a PWHT at 800°C due to a microstructure of fine-grained ferrite with fine dispersed carbide particles — Fig. 13C. The PWHT at 840°C increases the grain size and coarsens the carbide particles but produces the brittle fresh martensite — Fig. 13D. The toughness decreases from the 800°C PWHT value.

Conclusions

The impact toughness of the HAZ for Grade 91 steel welds has been experimentally investigated via measured thermal cycles, Gleeble® simulations, and microstructural analysis. The as-welded multipass HAZ has a significant scatter in toughness due to variations in the Charpy notch location and path of fracture propagation. The cross-weld Charpy specimen gives a toughness value that can be attributed to contri-

butions by the weld metal, various HAZ regions, and the base metal. The microstructure evolution of various HAZ regions during PWHT has been investigated and used to explain toughness changes.

1. A 760°C for 2 h PWHT can significantly increase the cross-weld toughness of the HAZ.

2. The measured weld HAZ toughness can be understood using a linear additive model that employs as the inputs the toughness values of various HAZ regions reproduced on the Gleeble®.

3. The toughness of the CGHAZ recovers the slowest as a function of increasing PWHT temperature and remains low until a 730°C heat treatment. To guarantee an adequate HAZ toughness, a minimum PWHT temperature of 730°C for 2 h is recommended. This recommendation agrees with the ASME code required 732°C minimum tempering temperature for the base metal.

4. The upper bound temperature for HAZ toughness seems to be the A_{C1} temperature. Postweld heat treatment 20°C below the A_{C1} temperature for 2 h has produced the highest toughness and lowest hardness of all HAZ regions. Postweld heat treatment above the A_{C1} temperature for 2 h will result in the formation of fresh martensite, which decreases the toughness and increases the hardness of all HAZ regions.

Acknowledgments

This work has been financially sponsored by the Department of Energy NEUP program. Technical guidance by Dr. Richard Wright is also gratefully acknowledged.

References

1. Sikka, V. K., Ward, C. T., and Thomas, K. C. 1983. Modified 9Cr-1Mo steel — an improved alloy for steam generator application. *Ferritic Steels for High-Temperature Applications, Proceedings of the ASM International Conference on Production, Fabrication Properties, and Applications of Ferritic Steels for High Temperature Applications*, 65–84. Metals Park, Ohio: ASM International.

2. Sanderson, S. J. 1983. Mechanical properties of 9Cr1Mo steel. *Ferritic Steels for High-Temperature Applications, Proceedings of the ASM International Conference on Production, Fabrication Properties, and Applications of Ferritic Steels for High Temperature Applications*, 85–99. Metals Park, Ohio: ASM International.

3. Pesicka, J., Kuzel, R., Dronhofer, A., and Eggeler, G. 2003. The evolution of dislocation density during heat treatment and creep of tempered martensite ferritic steels. *Acta Mater.* 51: 4847–4862.

4. Santella, M. L., Swinderman, R. W., Reed, R. W., and Tanzosh, J. M. 2010. *Martensite transformation, microsegregation, and creep strength of 9Cr-1Mo-V steel weld metal*. ORNL.

5. Sireesha, M., Albert, S. K., and Sundaresan, S. 2001. Microstructure and mechanical properties of weld fusion zones in modified 9Cr1Mo steel. *Journal of Materials Engineering and Performance* 10(3): 320–330.

6. Arivazhagan, B., Sundaresan, S., and Kamaraj, M. 2009. A study of influence of shielding gas composition on toughness of flux-cored arc weld of modified 9Cr-1Mo (P91) steel. *Journal of Materials Processing Technology* 209: 5245–5253.

7. Barnes, A. 1995. The influence of composition on microstructural development and toughness of modified 9Cr-1Mo weld metals. *Report 509/1995*. Abington, UK: TWI.

8. ASTM A370, *Standard Test Methods and Definitions for Mechanical Testing of Steel Products*.

9. LePera, F. S. 1980. Improved etching technique to emphasize martensite and bainite in high-strength dual-phase steel. *J. Met.* 32(3): 38, 39.

10. Moitra, A., Parameswaran, P., Sreenivasan, P. R., and Mannan, S. L. 2002. A toughness study of the weld heat-affected zone of a 9Cr-1Mo steel. *Materials Characterization* 48: 55–61.

11. Jang, Y. C., Hong, J. K., Park, J. H., Kim, D. W., and Lee, Y. 2007. Effect of notch position of the charpy impact specimen on the failure behavior in heat-affected zone. *Journal of Materials Processing Technology* 201: 419–424.

12. *Evaluation of Grade 91 Microstructure and Creep Rupture Strength as a Result of Heat Treatment Around the Intercritical Zone*. March 2009. EPRI Report 1015818. Palo Alto, Calif.

CAN WE TALK?

The *Welding Journal* staff encourages an exchange of ideas with you, our readers. If you'd like to ask a question, share an idea or voice an opinion, you can call, write, e-mail or fax. Staff e-mail addresses are listed below, along with a guide to help you interact with the right person.

Publisher
Andrew Cullison
cullison@aws.org, Extension 249
Article Submissions

Editor
Mary Ruth Johnsen
mjohnsen@aws.org, Extension 238
Feature Articles

Associate Editor
Howard Woodward
woodward@aws.org, Extension 244
Society News, Personnel

Associate Editor
Kristin Campbell
kcampbell@aws.org, Extension 257
New Products
News of the Industry

Managing Editor
Zaida Chavez
zaida@aws.org, Extension 265
Design and Production

Senior Production Coordinator
Brenda Flores
bflores@aws.org, Extension 330
Production

Advertising Sales Director
Rob Saltzstein
salty@aws.org, Extension 243
Advertising Sales

Advertising Sales & Promotion Coordinator
Lea Paneca
Lea@aws.org, Extension 220
Production and Promotion

Advertising Sales Representative
Sandra Jorgensen
sjorgensen@aws.org, Extension 254
Advertising Sales

Advertising Production Manager
Frank Wilson
fwilson@aws.org, Extension 465
Advertising Production

Peer Review Coordinator
Melissa Gomez
mgomez@aws.org, Extension 475
Peer Review of Research Papers

Welding Journal Dept.
8669 Doral Blvd. #130
Miami, FL 33166
(800) 443-9353
FAX (305) 443-7404